Nano Energy (2013) 2, 1010–1018

Available online at www.sciencedirect.com

ScienceDirect

journal homepage: www.elsevier.com/locate/nanoenergy

RAPID COMMUNICATION

Axial compressive α-Fe_2O_3 microdisks prepared from CSS template for potential anode materials of lithium ion batteries

Guo Gao[a,*], Qiang Zhang[b], Kan Wang[a], Hua Song[a], Peiyu Qiu[a], Daxiang Cui[a,*]

[a]*Department of Bio-Nano-Science and Engineering, Key Laboratory for Thin Film and Microfabrication of Ministry of Education, Institute of Micro-Nano Science and Technology, Shanghai Jiao Tong University, Shanghai 200240, China*

[b]*Beijing Key Laboratory of Green Reaction Engineering and Technology, Department of Chemical Engineering, Tsinghua University, Beijing 100084, China*

Received 21 February 2013; received in revised form 20 March 2013; accepted 21 March 2013
Available online 4 April 2013

KEYWORDS
α-Fe_2O_3;
Microdisks;
Hydrothermal;
Lithium ion battery;
Axial compressive

Abstract
In this paper, α-Fe_2O_3 microdisks (~1.1 μm in diameter, ~150 nm in thickness) have been synthesized by a facile hydrothermal method using a novel $NaNO_3$-Na_2SO_4 crystal salts solution (CSS) containing CNTs fragments as template. Interestingly, the synthesized α-Fe_2O_3 microdisks exhibit a unique axial compressive property. The small-sized CNTs fragments in α-Fe_2O_3 microdisks could act as a robust framework for such assemblies and endow them the axial compressive property. Owing to the existence of CNTs fragments, the α-Fe_2O_3 microdisks are not easily destroyed. AFM results indicate that the α-Fe_2O_3 microdisks could be compressed to 10–50 times than the original thickness. Electrochemical studies show that the synthesized α-Fe_2O_3 microdisks exhibited good cyclic stability and rate performance. The α-Fe_2O_3 microdisks electrode delivers a reversible specific capacity of 632 mA h g^{-1} even at a high rate of 800 mA g^{-1}. When returning to the initial rate of 100 mA g^{-1}, the α-Fe_2O_3 microdisks electrode returns to a higher capacity (968 mA h g^{-1}). The unique axial compressive property of α-Fe_2O_3 microdisks endows that they could alleviate the pulverization and structural destruction of electrodes during the lithium ion insertion and extraction process.

Introduction

Since the first commercialization by Sony Corporation in the early 1990s, lithium ion batteries (LIBs) are becoming the predominant power source for portable electronic and electric

*Corresponding authors. Tel: +862134206962.
E-mail addresses: gaogaoguoguo@yahoo.com.cn (G. Gao), dxcui@sjtu.edu.cn (D. Cui).

2211-2855/$ - see front matter © 2013 Elsevier Ltd. All rights reserved.
http://dx.doi.org/10.1016/j.nanoen.2013.03.023

vehicles due to their high energy density, long lifespan, fast charge-discharge rate and durable cycling performance [1,2]. Developing novel powder materials for producing and storing electricity is a key issue to meet the increasing energy demand. Among the reported active materials for LIBs, iron oxides show high capacity, low cost, natural abundance, safety (a slightly higher voltage plateau) and environmental benignity [3,4]. Compared with the capacity of available electrode materials (urchin-like CuO, $>560\ mA\ h\ g^{-1}$; graphite $<372\ mA\ h\ g^{-1}$; $Li_4Ti_5O_{12}$, 161.9 $mA\ h\ g^{-1}$; $NiSi_2$, 600 $mA\ h\ g^{-1}$), iron oxides have been becoming the most promising candidates for Li batteries because of their high theoretical capacity (Fe_3O_4, ~928 $mA\ h\ g^{-1}$; Fe_2O_3, 1005 $mA\ h\ g^{-1}$), resulting in the formation of a Li_2O buffering matrix on electrochemical reaction or favorable crystal structure for lithium insertion [5-8].

Hematite (Fe_2O_3) is an n-type semiconductor (band gap of 2.1 eV) and has antiferromagnetic properties [9]. As for anode materials of LIBs, lithium storage mechanism of Fe_2O_3 is attributed to a redox conversion reaction ($Fe_2O_3 + 6Li^+ + 6e^- \leftrightarrow 2Fe + 3Li_2O$), where the hematite is reduced to Fe nanograins dispersed in Li_2O matrix upon lithiation and then reversibly restored to their initial oxidation states during delithiation. Generally, the capacity of transition metal oxides (MO, M=Fe, Co, Ni, Mn or Cu) is not only related with their natural properties but also related to their structures. [10,11,29] Therefore, designing and tailoring the architectures of iron oxides with desired shapes have attracted considerable interests in the scientific and industrial fields. For the past several years, intensive research has been devoted to the controllable synthesis of iron oxides nanomaterials with different shapes. Muraliganth et al. [12] reported the microwave-hydrothermal method for synthesis of Fe_3O_4 nanowires. Nuli and co-workers [13] reported a hydrothermal method for the synthesis of α-Fe_2O_3 with different morphologies (e.g., cubic, spherical, sheet-like and rod-like). Mitra et al. [14] reported a solvothermal route for synthesis of nanospindle, nanorhombohedron and nanocube structured α-Fe_2O_3. According to the diffusion equation $\boldsymbol{t}=\boldsymbol{L}^2/2\boldsymbol{D}$ ($\boldsymbol{t}$, diffusion time; $\boldsymbol{L}$, diffusion distance; $\boldsymbol{D}$, diffusion coefficient), it can be deduced that decreasing the particles sizes could shorten the diffusion time of Li in iron oxides and significantly improve the powder electrochemical performance [15]. Therefore, iron oxides with hollow nanostructures or thin sheets structures are the promising candidates for anode materials of LIBs [16,17]. Such structures could provide large contact area for higher Li^+ diffusion between the electrode and electrolyte, and absorb and store numerous lithium ions. Furthermore, such structures could offer faster diffusion for Li^+ uptake/removal as compared with solid nanoparticles and better tolerate for the volume variation and severe particles aggregation during the repeated charge-discharge cycling. Here, α-Fe_2O_3 microdisks (~1.1 μm in diameter, ~150 nm in thickness) have been successfully synthesized by a novel hydrothermal process using a novel $NaNO_3$-Na_2SO_4 crystal salts solution (CSS) containing CNTs fragments as template. The small-sized CNTs fragments in α-Fe_2O_3 microdisks could act as a robust framework for such assemblies and endow them the axial compressive property. The α-Fe_2O_3 microdisks have a thin sheet structure that (1) allows the electrolyte to penetrate inside the substrates, resulting in high accessibility of the active materials, (2) promotes the fast lithium diffusion because of the short lithium pathway within the microdisks, and (3) improves the electron conductivity and enhances cyclic stability/rate capability. Although, disk-like α-Fe_2O_3 has been synthesized by a top-down strategy, however, to the best of our knowledge, as of yet there has been no report on using CSS as the template to synthesize α-Fe_2O_3 microdisks with such special axial compressive property as anode materials for lithium ions batteries.

Material and methods

Synthesis of $NaNO_3$-Na_2SO_4 crystal salts solution

The $NaNO_3$-Na_2SO_4 crystal salts solution (CSS) was obtained by the following procedure: (1) double helix carbon nanotubes (CNTs) were synthesized according to our previous reported procedure [26]. (2) 0.3 g CNTs were then oxidized by nitric acid and sulfuric acid in the ratio of 1:3 in a Teflon cell at 105 °C for 30 min. (3) After oxidation reaction, the pH value of mixed solution was adjusted to 7.5-8.5 using sodium hydroxide. Then, the obtained solution was centrifuged at 9500 r/m for 15 min. The upper clean solution was the $NaNO_3$-Na_2SO_4 crystal salts solution. The samples for SEM images were prepared via dropping 2 μL CSS solution on a silica surface, and dried naturally at room temperature.

Synthesis of α-Fe_2O_3 microdisks

Monodisperse α-Fe_2O_3 microdisks were synthesized by a hydrothermal process in the presence of $NaNO_3$-Na_2SO_4 crystal salts solution. In a typical synthesis procedure, 1.11 g $FeSO_4 \cdot 7H_2O$ was dissolved in 20 mL above-mentioned crystal salts solution. Then 15 mL NaOH solution (0.2 M) was gradually added. After stirring for 20 min, the mixed solution was transferred into a Teflon-lined autoclave and heated to 200 °C for 10 h. After reaction, brick red uniform α-Fe_2O_3 microdisks can be obtained in a large scale.

Characterization of α-Fe_2O_3 microdisks

The crystal structure and sizes were characterized by scanning electron microscopy (SEM, FEI-Sirion 200), transmission electron microscopy (TEM, JEM-2010), high-resolution transmission microscopy (HRTEM) and selected area electron diffraction (SAED). Samples compositions were characterized by an X-ray diffractometer (XRD, Rigaku, Japan) using Cu Kα radiation at 1.5418 Å at a scanning rate of 5°/min. The axial compressive property of α-Fe_2O_3 microdisks has been investigated by atomic force microscopy (AFM, E-Sweep) using magnetic tip.

Lithium storage performance measurements

α-Fe_2O_3 microdisks were evaluated as anode materials for lithium ion cells by galvanostatic charge-discharge technique. The electrode was prepared by mixing the active materials, acetylene black and polyvinylidene fluoride (PVDF) with weight ratios of 80:10:10 in ***N***-methyl-2-pyrrolidone solvent, which was then coated on a copper foil, pressed and dried at

120 °C for 12 h in a vacuum drying oven. Coin cells were assembled in an argon-filled glovebox in the presence of oxygen scavenger and sodium drying agent. Iron oxides composites act as test electrode, metallic lithium as counter/reference electrode, 1 M LiPF6 in ethylene carbonate, diethyl carbonate and ethylmethyl carbonate (EC/DMC/EMC, 1:1:1 vol) electrolyte, and Celgard 2400 polypropylene as separator. Charge-discharge tests were carried out at various densities at the voltage range of 0.002-3.0 V (vs Li/Li^+) using a battery test system (BTSDA 7.0).

Results and discussion

Characterization of α-Fe_2O_3 microdisks

Fig. 1a shows that the synthesized α-Fe_2O_3 microdisks are monodispersed. The shape of α-Fe_2O_3 is disk-like structure. The diameter of microdisks is about 1.1 μm, and the thickness is about ~150 nm (Fig. 1b). In fact, the α-Fe_2O_3 microdisks were built by a lot of thin nanosheets, and these nanosheets fused together, forming the microdisk architecture with multi-layer structure (Fig. 1c). In our experiment, the α-Fe_2O_3 microdisks can be obtained in a large quantity (Fig. 1d). The TEM image in Fig. 2a shows the regular microdisks shape of the α-Fe_2O_3 powders. The edge of microdisks is constructed by numerous thin sheets (Fig. 2b). Clear and continuous lattice-fringe images can be observed in Fig. 2c. The distance of neighboring fringes was measured to be 0.253 nm, close to that of (110) lattice spacing (0.251 nm) in α-Fe_2O_3 structure. From the high resolution TEM image, it is clearly seen that the synthesized α-Fe_2O_3 microdisks have high crystalline. The selected area electron diffraction (SAED) in Fig. 2d also reveals that the microdisks have high crystalline. The X-ray diffraction (XRD, D8 Advance, Bruker-Axs) pattern (Fig. S1) of the synthesized α-Fe_2O_3 microdisks shows a typical reflection pattern of the rhombohedral hematite Fe_2O_3 structure (JCPDS No.1-1053).

Electrochemical performance for LIBs

To assess the potential of α-Fe_2O_3 microdisks for anode materials of LIBs, we conducted electrochemical tests using coin cells (CR 2025). Fig. 3a shows the discharge-charge profiles of the α-Fe_2O_3 microdisks electrode for the 1st, 2nd, 10th, 40th and 50th cycle at a rate of 85 mA g^{-1} in the voltage range from 0.002 to 3.0 V (vs Li/Li^+). As for the 1st cycle, the discharge curve reached a voltage plateau at about 1.68 V and then a 0.86 V plateau followed by a long slope. The two voltage plateau can be attributed to the formation of solid electrolyte interphase (SEI) film on the surface of electrode and the insertion of lithium ions into the α-Fe_2O_3 microdisks electrode. The discharge capacity of α-Fe_2O_3 microdisks electrode in the 1st, 2nd, 10th, 40th and 50th cycle is 1284, 901, 844, 899 and 910 mA h g^{-1}, respectively. For the prepared α-Fe_2O_3 microdisks, the first discharge capacity was found to be around 1284 mA h g^{-1}, corresponding to the insertion of about 11 Li per α-Fe_2O_3 formula. In the second discharge, the capacity decreases to 901 mA h g^{-1}. This is attributed to the formation of SEI film and further lithium consumption via interfacial reactions due to the charge separation at the metal/Li_2O phase boundary. [18] During the following cycles, the average voltage plateau of discharge process maintains about 0.95 V. The voltage plateau at 0.95 V in the following cycle is different with the first cycle at 0.86 V, suggesting that irreversible reactions occurred in the first cycle. In the charge process, the charge capacity of α-Fe_2O_3 microdisks electrode in the 1st, 2nd, 10th, 40th and 50th cycle is 847, 822, 805, 857 and 874 mA h g^{-1}, respectively. For the first charge process, only 7 Li could be removed reversibly owing to the charge capacity of 847 mA h g^{-1}. After the 40th cycle, the discharge and charge curves nearly overlap, indicating that the α-Fe_2O_3 microdisks electrode has a good cyclic stability. It is known that commercial graphite has the risk of high-surface-area Li plating at the end of recharge, which is related to the safety problems [19]. As for the synthesized α-Fe_2O_3 microdisks

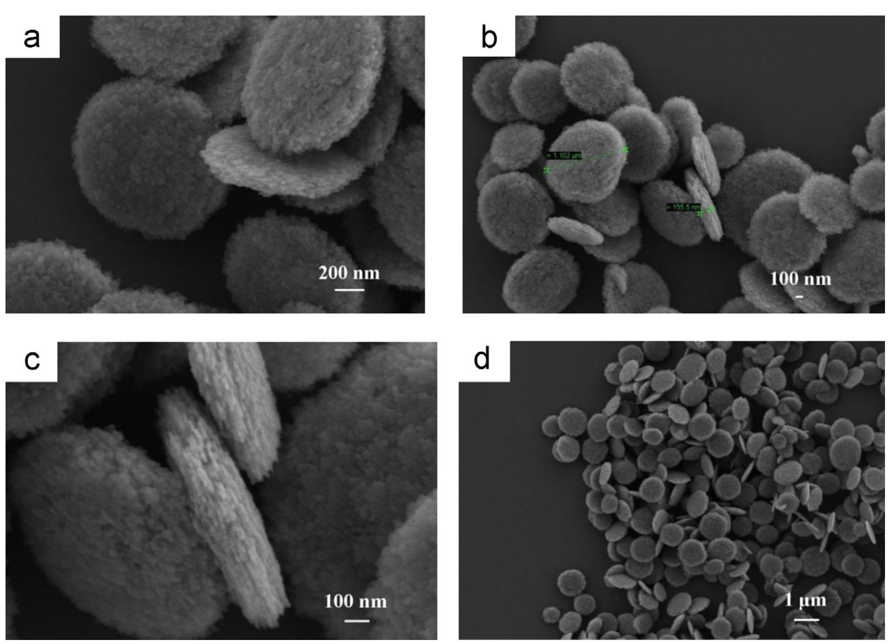

Fig. 1 SEM images of the synthesized α-Fe_2O_3 microdisks (a-d).

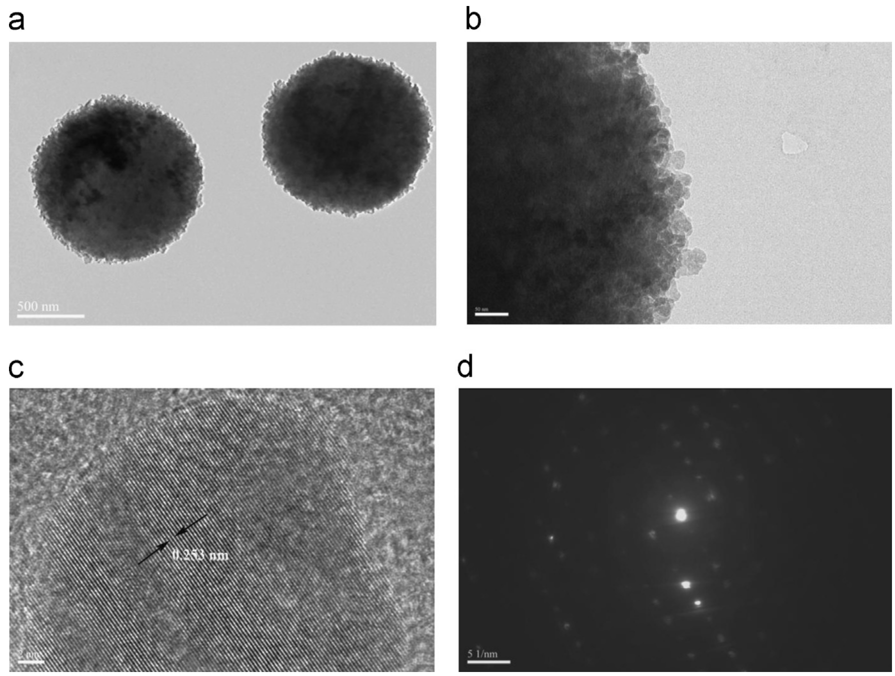

Fig. 2 TEM images (a-b), HRTEM (c), and SAED pattern (d) of the α-Fe_2O_3 microdisks.

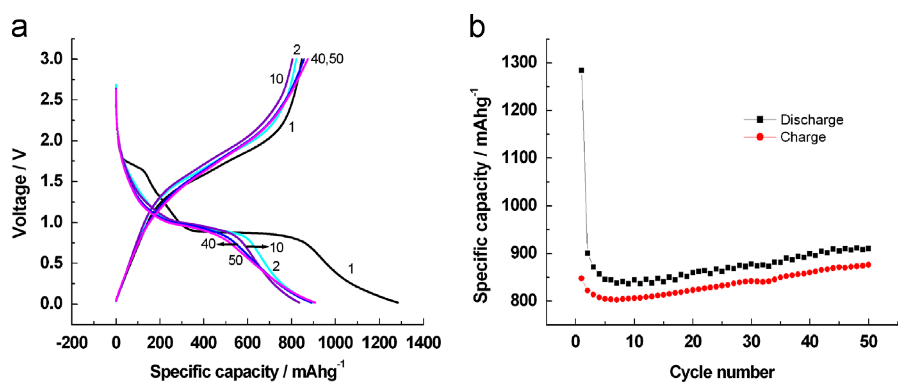

Fig. 3 Discharge-charge curves (a), and cycling stability (b) of the synthesized α-Fe_2O_3 microdisks.

electrode, it will reduce the risk because of its higher voltage plateau. The cyclic performance of α-Fe_2O_3 microdisks in 0.002–3.0 V (vs Li/Li^+) is shown in Fig. 3b. The results indicate that the discharge capacity of α-Fe_2O_3 microdisks electrode in the first cycle is as high as 1284 mA h g^{-1} and corresponding charge capacity is 847 mA h g^{-1} at a 85 m Ag^{-1} rate, which exceed the theoretical value of Fe_2O_3 (1005 mA h g^{-1}). This is possibly attributed to the electrolyte decomposition, lithium storage on the surface of polymeric layer or interfacial storage [20]. More importantly, we note that the discharge capacity and charge capacity have an increase trend after the 10th cycle. This phenomenon might be attributed to the activation and stabilization of electrode materials. After 10th cycle, the discharge capacity increases from 844 mA h g^{-1} to 860 (20th), 878 (30th), 899 (40th) and 910 (50th) mA h g^{-1}, respectively. High discharge capacity of 910 mA h g^{-1} and charge capacity of 874 mA h g^{-1} can be retained for the α-Fe_2O_3 microdisks electrode after 50 cycles. This means that the α-Fe_2O_3 microdisks could promote the fast lithium diffusion and enhance cyclic stability because of the short lithium pathway within the microdisks.

Besides their high capacity, the synthesized α-Fe_2O_3 microdisks also exhibit good rate capability. Fig. 4a shows the cycling of α-Fe_2O_3 microdisks electrode at continuously various rates for the same battery. At a rate of 100 mA g^{-1}, a capacity of 859 mA h g^{-1} is obtained. At 200, 400 and 600 mA g^{-1}, the capacity drops to 815, 755 and 702 mA h g^{-1}, respectively. Though the capacity drops, it remains stable after 11 cycles. Clearly, the electrode delivers a reversible specific capacity of 632 mA h g^{-1} even at a high rate of 800 mA g^{-1}. When returning to the initial rate of 100 mA g^{-1}, the α-Fe_2O_3 microdisks electrode returns to a higher capacity (968 mA h g^{-1}) than the original capacity (859 mA h g^{-1}). The results confirm that the α-Fe_2O_3 microdisks electrode can keep its integrity during the discharge-charge process, which exhibit the good dynamic performance. Fig. 4b shows the first discharge-charge curves at different rates for the α-Fe_2O_3 microdisks electrode. Clearly, the capacity gradually

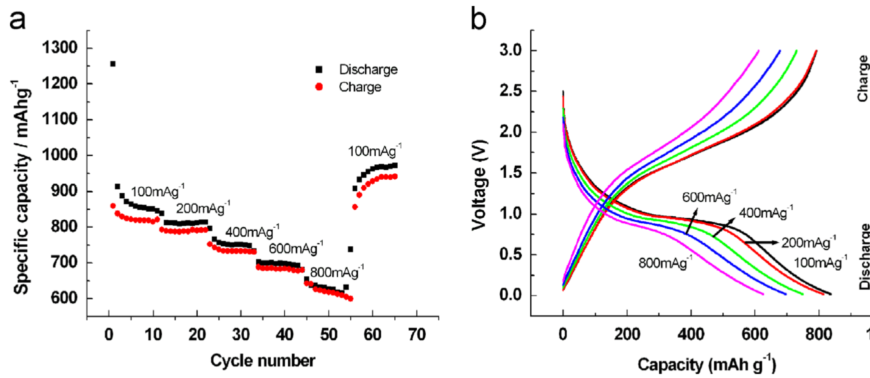

Fig. 4 Cycling performance of the same cell at various rates (a), and first discharge-charge curves at different rates (b) for α-Fe_2O_3 microdisks electrode.

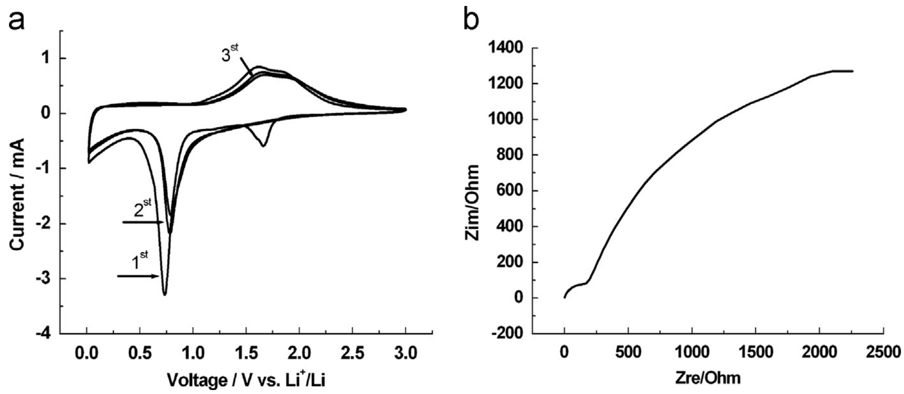

Fig. 5 Cyclic voltammograms (a) and Nyquist plots of ac impedance spectra collected in the frequency range between 10 mHz and 100 kHz after three CV cycles (b) for the α-Fe_2O_3 microdisks. Note that the initial three cycles at a scan rate of 0.1 mV s^{-1}.

degrades with the increase of current density. At rate of 100 mA g^{-1}, the first discharge capacity is around 833 mA h g^{-1}, corresponding to the insertion of almost 7 Li per Fe_2O_3. At higher rate of 800 mA g^{-1}, the insertion of 5 Li per Fe_2O_3 formula is found.

Fig. 5a shows the cyclic voltammogram (CV) curves of the α-Fe_2O_3 microdisks electrode for the initial three cycles at a rate of 0.1 mV s^{-1}. It is clear that there is a substantial difference between the first and the subsequent cycles. In the cathodic process of the 1st cycle, two peaks, a bulky peak and a tiny peak, are observed at about 0.72 and 1.66 V. This can be attributed to the lithium intercalation in the crystal structure of Fe_2O_3 microdisks, the chemical reduction reaction of Fe^{3+} or Fe^{2+} to Fe^0 and the irreversible reaction with the electrolyte [21,22]. In this step, the conversion of Fe_2O_3 to Fe and the formation of amorphous Li_2O are the main cause of the irreversible capacity during the discharge step [23]. In the anodic process, two broad peaks located at 1.61 and 1.86 V are observed, corresponding to the oxidation reaction of Fe^0 to Fe^{2+} and Fe^{2+} to Fe^{3+} [24]. In the 2nd and 3rd cycles, only one peak located at 0.78 V is observed in the cathodic process, suggesting an irreversible phase transformation occurred during lithium ion intercalation and extraction in the 1st cycle [25]. During the subsequent cycles, the intensity of cathodic and anodic peaks compared to the first cycle decreases gradually. This implies that the capacity decreases during the cycling. In addition we note that the reduction peak is shifted from 0.72 V to a higher potential of 0.78 V, whereas the oxidation peak position and integrated area remain nearly unchanged, revealing the good reversibility reaction from the Fe^0 to Fe^{3+} and a low capacity loss of lithium insertion and extraction after the first cycle. Fig. 5b shows the Nyquist plots of cell after three cyclic voltammetry cycles. The Nyquist plots at high frequency have a semicircle in the complex plane, with the center under the real axis, which is a typical behavior for solid electrodes with the frequency dispersion of impedance data [30,31]. The impedance complex plane plots are similar to a depressed semicircular shape, suggesting that a homogeneous film is formed on the surface of electrode. In the high frequency range, the electrochemical process can be described for the film capacitance and film resistance. In the low frequency range, the electrochemical process is related to the charge transfer resistance and the double layer capacitance in the electrode/electrolyte interface. Generally, a constant phase element was used instead of an ideal capacitance, revealing all the non-ideal frequency-dependent electrochemical phenomena.

Formation mechanism of α-Fe_2O_3 microdisks

The electrochemical measurements show that the α-Fe_2O_3 microdisks exhibit good cyclic stability. The α-Fe_2O_3 microdisks have a thin sheet structure, which may easily shorten the diffusion time of Li in iron oxides. Also, the small amounts of CNTs fragments in α-Fe_2O_3 microdisks will significantly improve the powder electrochemical performance. As for the formation mechanism of α-Fe_2O_3 microdisks, their growth process at different stages has been investigated. In our experiment, the $NaNO_3$-Na_2SO_4 crystal salts solution (CSS) was obtained by firstly oxidizing double helix CNTs, and then centrifuging the solution at 9500 r/m. The morphology of the synthesized CNTs can be seen in Fig. S2. As for α-Fe_2O_3 microdisks, the CSS must play an important role through this process. During the addition of sodium hydroxide, the temperature of initial solution nearly reached to 80 °C. When the pH value was adjusted to 7.5–8.5, the solution was then gradually cooled to room temperature. At this stage, some crystalline salts are evolved and precipitated. Therefore the CSS was, in fact, a supersaturated solution. When the CSS solution was dropped on a silica surface, and dried naturally at room temperature, the $NaNO_3$-Na_2SO_4 crystal salts solution have a tendency to form numerous dispersed snow-like aggregates (Fig. S3, S4) via crystallization through the evaporation of solvent, and each aggregate was constructed by some tree-structured branches. These branches are aggregated together at a common center, forming a snow-like architecture. The diameter of $NaNO_3$-Na_2SO_4 crystal salts can reach ~100 μm. The evolved crystal salts in CSS solution was identified to the mixed compositions of $NaNO_3$-Na_2SO_4 (Fig. S5). In the CSS system, there is a negative charge on the surface of CNTs fragments. When Fe^{2+} ions were added, these Fe^{2+} ions are easily adsorbed on the surface of CNTs fragments by the charge interaction. These CNTs fragments could act as 'in situ' soft templates for accepting Fe^{2+} ions. Because Fe^{2+} ions are all captured by CNTs fragments, they can effectively prevent the agglomeration tendency of Fe^{2+} precipitates during the nucleation process. Because the CSS solution is a supersaturated solution, the crystallization process will rapidly occur when there are ample Fe^{2+} precipitates nuclei. CSS is homogeneous system, and it has a tendency to form a snow-like architecture during crystallization process. These special properties of CSS may promote the formation of disk-like precursors for α-Fe_2O_3 microdisks. The precursors were composed of CNTs fragments, $NaNO_3$-Na_2SO_4 crystal salts and Fe^{2+} precipitates. With the increase of reaction temperature, Fe^{2+} precipitates are gradually converted into the growing Fe_2O_3 nanoparticles. At the same time, crystal salts in the precursors were gradually dissolved. To minimize the overall energy of system, the crystal salts will dissolve from the outer surface to inner part, leaving some void spaces in the precursors. Owing to the existence of small-sized CNTs fragments, the decomposition and dissolution process of precursors will not lead to the disassembly of framework structure. After reacting at 200 °C for 10 h, axial compressive α-Fe_2O_3 microdisks were formed.

In fact, the oxidation process of CNTs is very important for the synthesis of α-Fe_2O_3 microdisks because CNTs may provide some small-sized CNTs fragments which are acting as the framework for α-Fe_2O_3 microdisks. Since CSS was centrifuged at 9500 r/m for 15 min, bigger CNTs fragments were completely removed. There are still some remanet CNTs fragments in the crystal salts solution. No XRD diffraction peaks at 28.93° and 41.16° were observed, confirming the amount of CNTs fragments in the α-Fe_2O_3 microdisks are low. Fourier transform infrared (FTIR, Nicolet 6700, ThermoFisher) analysis (Fig. S6) of α-Fe_2O_3 microdisks was carried out at 4000–400 cm^{-1}. In the range of 400–700 cm^{-1}, it can be seen that α-Fe_2O_3 microdisks have two characteristic peaks at 476.7 cm^{-1} and 547.1 cm^{-1}. The absorption peak at 476.7 cm^{-1} was attributed to the perpendicular modes of the Fe–O stretching vibrations in the corundum structure [27]. Other absorption peaks at 3446.2, 1640, 1389 and 1125.7 cm^{-1} confirm the presence of a few CNTs fragments in the α-Fe_2O_3 microdisks. In order to confirm the presence of CNTs in the α-Fe_2O_3 microdisks, we carried out the X-ray photoelectron spectra (XPS) analysis (Fig. S7). The C1s binding energies (Fig. S8) are 284.7 eV, 288.4 eV and 289.5 eV, which correspond to C–C/C–H, carbonyl groups and carboxyl groups, respectively, clearly indicate that the presence of a few remanet CNTs oxidation fragments in the α-Fe_2O_3 microdisks. The O1s spectra (Fig. S9) show the presence of three states of oxygen in the samples. The peak at 529.9 eV was assigned to O^{2-} in the iron oxide lattice. The binding energies located at 531.8 eV and 532.9 eV can be attributed to the OH^- or adsorption oxygen. The characteristic peaks of Fe2p (Fig. S10) at 710.8 eV and, 720.6 eV and 724.5 eV well agreed with the Fe^{3+} state for iron oxides [28]. The presence of small-sized CNTs fragments in α-Fe_2O_3 microdisks hints that these CNTs fragments act as the initial framework role for the formation of disk-like Fe_2O_3.

Interestingly, we observed that the magnetic force (magnetic tip was used in the AFM tests) of atomic force microscopy (AFM) could significantly influence the thickness of the synthesized α-Fe_2O_3 microdisks. This means that the synthesized α-Fe_2O_3 microdisks have an axial compressive property which can provide a cushion space for the volume changes for LIBs during charges–discharges process. This special property of α-Fe_2O_3 microdisks may be hopefully applied in the LIBs, medical diagnosis and biological area. Fig. 6a shows the AFM image of α-Fe_2O_3 microdisks in the use of common tip. The samples are smooth and have a well-defined edge, presenting a typical disk-like structure. The α-Fe_2O_3 microdisks evenly covered the mica thin slip surface. The diameter of α-Fe_2O_3 microdisks is ~1 μm, and height is ~200 nm. When the magnetic tip was used (the first scan for α-Fe_2O_3 microdisk), the height of microdisks decreases significantly (Fig. 6b). The maximum height is ~20 nm and the minimum height is ~4 nm, whereas the diameter is still ~1 μm. The corresponding planar image in Fig. 6c clearly shows that the maximum height for a given α-Fe_2O_3 microdisk only takes about half area. In order to monitor the height variation between the microdisk and scan times, we carried out a real-time observation study (Fig. S11). As for the 2nd, 3rd, 6th, 8th, 10th and 16th scan for a fixed-area image (Fig. 6d–i), the area for maximum height of α-Fe_2O_3 microdisks decreases with the scan times. The area of maximum height decreases very quickly before the 8th scan, and becomes slowly after that (Fig. 7). This evolution indicates that the synthesized α-Fe_2O_3 microdisks have an axial compressive property. In order to verify the stability of α-Fe_2O_3 microdisks as anode materials originated from this effect, SEM images (Fig. S12) of α-Fe_2O_3 microdisks electrode after cycling at a rate of 100 mA g^{-1} indicate that the α-Fe_2O_3 microdisks maintain their shapes well. Although, the sizes of α-Fe_2O_3 microdisks are relatively bigger to use as anode materials, they were in fact not broken into small pieces which reacted with lithium due to their axial compressive property. When magnetic force was applied, the α-Fe_2O_3 microdisks could be compressed 10–50 times than the original thickness. This unique axial compressive property of α-Fe_2O_3 microdisks endows that they could alleviate the pulverization and structural destruction of electrodes during the lithium ion insertion and extraction process, and exhibit good cyclic stability and rate performance. Therefore,

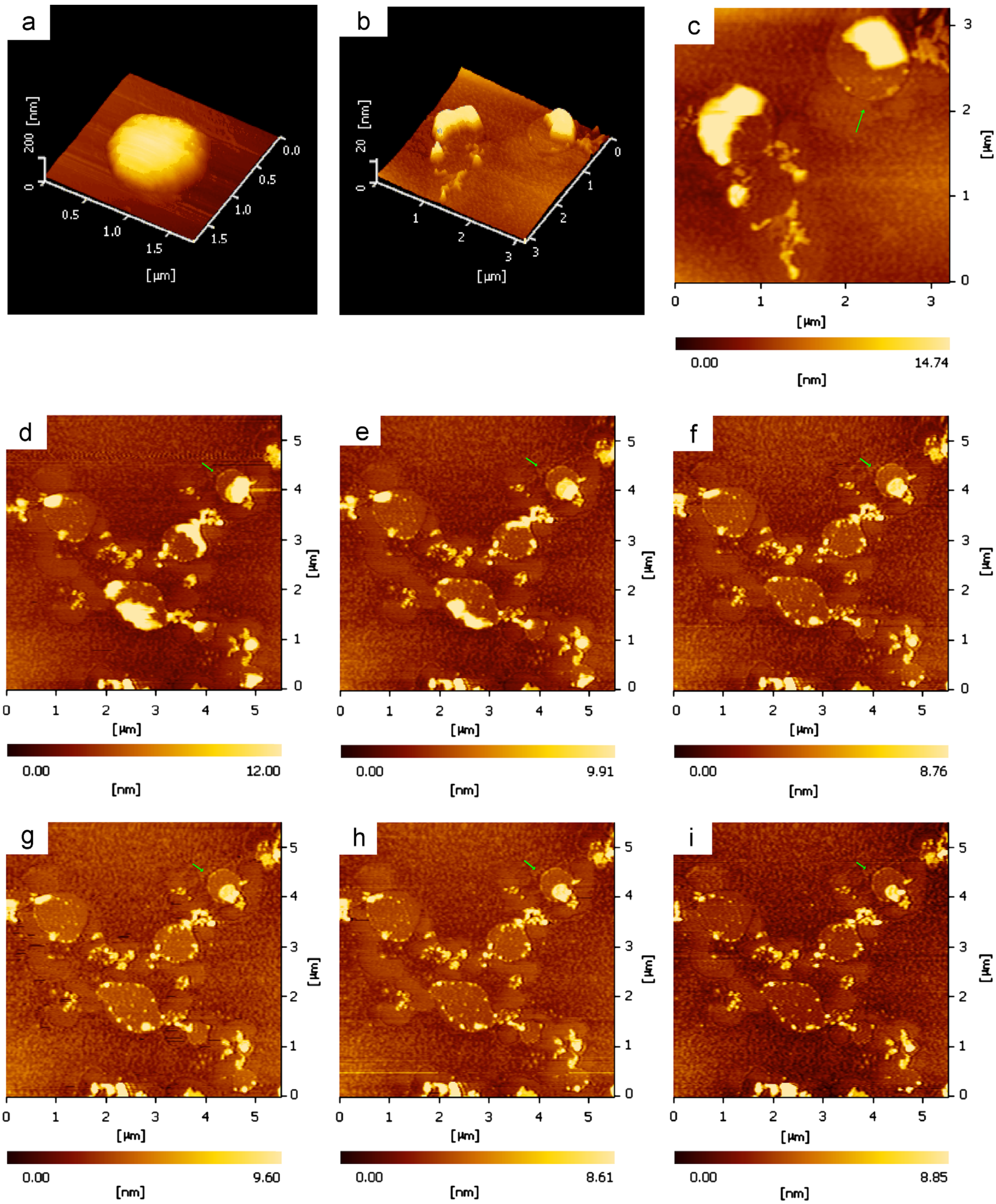

Fig. 6 AFM image of α-Fe_2O_3 microdisks without the use of magnetic tip (a), 1st scan 3-D image (b), and planar image (c) using the magnetic tip, the 2nd (d), 3rd (e), 6th (f), 8th (g), 10th (h), and 16th (i) planar scan image at a fixed-area using the magnetic tip.

the electrochemical properties of α-Fe_2O_3 microdisks can be explained as follows: first, α-Fe_2O_3 microdisks have high reactivity with lithium ion insertion and extraction process, and at the same time alleviate the absolute volume changes. Second, the disk-like structure of α-Fe_2O_3 provide large contact area and good adherence between Fe_2O_3 and carbon matrix, which decreases the diffusion distance of lithium ions and promotes the electron/lithium ions conduction. Finally, small amount of CNTs fragments in the α-Fe_2O_3 microdisks may catalyze the reversible transfer of Li_2O and improve the electron and ions conduction networks. Our thermogravimetric analysis (TGA) shows that the small amount of CNTs fragments accounts to about 1.2 wt% in the samples of α-Fe_2O_3 microdisks (Fig. S13). The existence of spaces in α-Fe_2O_3 microdisks was

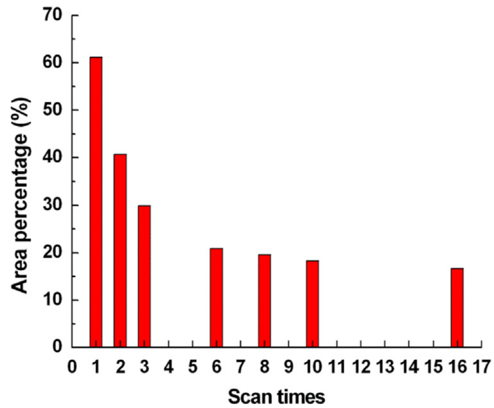

Fig. 7 The relationship between the area percentage of maximum height and scan times based on the AFM images. Area percentage (%) = 100×the area of maximum height/total area for a given microdisk (arrow). The area was calculated by an Image-Pro Plus software.

identified by our SEM images (Fig. S14) after the samples were washed with small amounts of dilute sulfuric acid. In order to verify the existence of short CNTs in the α-Fe_2O_3 microdisks, we have carefully observed the boundary edge of microdisks and found the existence of short CNTs fragments (Fig. S15). When the α-Fe_2O_3 microdisks were thoroughly dissolved by dilute sulfuric acid, the existence of trace amount of CNTs fragments was confirmed (Fig. S16).

Conclusions

In conclusion, axial compressive α-Fe_2O_3 microdisks (~1.1 μm in diameter, ~150 nm in thickness) with good electrochemical properties have been successfully synthesized by a novel hydrothermal method. The α-Fe_2O_3 microdisks electrode delivers a reversible specific capacity of 632 mA h g^{-1} even at a high rate of 800 mA g^{-1}. When returning to the initial rate of 100 mA g^{-1}, the α-Fe_2O_3 microdisks electrode returns to a higher capacity (968 mA h g^{-1}). The unique axial compressive property of α-Fe_2O_3 microdisks endows that they could alleviate the pulverization and structural destruction of electrodes during the lithium ion insertion and extraction process. We believe that further optimization of the size and morphology of α-Fe_2O_3 microdisks can further improve the electrochemical performance.

Acknowledgments

We thank the financial support by Chinese 973 Project (2010CB933901 and 2011CB933100), National Natural Science Foundation of China (nos. 81225010, 81101169, 31100717, 31170961), New Century Excellent Talent of Ministry of Education of China (NCET-08-0350), Shanghai Science and Technology Fund (1052nm04100), Important National Science & Technology Specific Projects (2009ZX10004-311) and Specialized Research Fund for the Doctoral Program of Higher Education (no. 20110073120072). Authors are also grateful for the Instrumental Analytical Center of Shanghai Jiao Tong University.

Appendix A. Supporting information

Supplementary data associated with this article can be found in the online version at http://dx.doi.org/10.1016/j.nanoen.2013.03.023.

References

[1] (a) J.M. Tarascon, M. Armand, Nature 414 (2001) 359;
b) B. Scrosati, J. Hassoun, Y.K. Sun, Energy and Environmental Science 4 (2011) 3287;
(c) V. Etacheri, R. Marom, R. Elazari, G. Salitra, D. Aurbach, Energy and Environmental Science 4 (2011) 3243;
(d) X.H. Liu, J.Y. Huang, Energy and Environmental Science 4 (2011) 3844.
[2] C.K. Chan, H.L. Peng, G. Liu, K. McIlwrath, X.F. Zhang, R.A. Huggins, Y. Cui, Nature Nanotechnology 3 (2008) 31.
[3] C. Yang, J. Wu, Y. Hou, Chemical Communication 47 (2011) 5130.
[4] Q. Qu, S. Yang, X. Feng, Advanced Materials 23 (2011) 5574.
[5] T. Pedro, P.M. Maria, G.C. Teresita, V.V. Sabino, J.S. Carlos, Advanced Materials 23 (2011) 5243.
[6] L. Taberna, S. Mitra, P. Poizot, P. Simon, J.M. Tarascon, Nature Materials 5 (2006) 567.
[7] H. Liu, G. Wang, J. Park, J. Wang, H. Liu, C. Zhang, Electrochimica Acta 54 (2009) 1733.
[8] J. Su, M. Cao, L. Ren, C. Hu, Journal of Physical Chemistry C 115 (2011) 14469.
[9] A.G. Nasibulin, S. Rackauskas, H. Jiang, Y. Tian, P.R. Mudimela, S.D. Shandakov, L.I. Nasibulina, J. Sainio, E.I. Kauppinen, Nano Research 2 (2009) 373.
[10] W. Wang, M. Tian, A. Abdulagatov, S.M. George, Y.C. Lee, R. Yang, Nano Letters 12 (2012) 655.
[11] Y. Li, B. Tan, Y. Wu, Nano Letters 8 (2008) 265.
[12] T. Muraliganth, A.V. Murugan, A. Manthiram, Chemical Communication 47 (2009) 7360.
[13] Y. Nuli, R. Zeng, P. Zhang, Z. Guo, H. Liu, Journal of Power Sources 184 (2008) 456.
[14] S. Mitra, S. Das, K. Mandal, S. Chaudhuri, Nanotechnology 18 (2007) 275608.
[15] X.L. Xu, L.Y. Jiang, F.F. Cao, Y.G. Guo, L.J. Wan, Advanced Materials 21 (2009) 2710.
[16] B. Koo, H. Xiong, M.D. Slater, V.B. Prakapenka, M. Balasubramanian, P. Podsiadlo, C.S. Johnson, T. Rajh, E.V. Shevchenko, Nano Letters 12 (2012) 2429.
[17] (a) Z. Wang, L. Zhou, X.W. Lou, Advanced Materials 24 (2012) 1903;
(b) B. Wang, J.S. Chen, H.B. Wu, Z. Wang, X.W. Lou, Journal of the American Chemical Society 133 (2011) 17146;
(c) J.S. Chen, T. Zhu, X.H. Yang, H.G. Yang, X.W. Lou, Journal of the American Chemical Society 132 (2010) 13162.
[18] J. Jamnik, J. Maier, Physical Chemistry Chemical Physics 5 (2003) 5215.
[19] J.M. Tarascon, M. Armand, Nature 414 (2001) 359.
[20] M.R. Palacin, J. Cabana, L. Monconduit, D. Larcher, Advanced Materials 22 (2010) E170.
[21] G. Zhou, D.W. Wang, F. Li, L. Zhang, N. Li, Z.S. Wu, L. Wen, G.Q. Lu, H.M. Cheng, Chemistry of Materials 22 (2010) 5306.
[22] W.J. Yu, P.X. Hou, F. Li, C. Liu, Journal of Materials Chemistry 22 (2012) 13756.
[23] H. Liu, G. Wang, J. Wang, D. Wexler, Electrochemical Communication 10 (2008) 1879.
[24] J. Morales, L. Sanchez, F. Martin, F. Berry, X. Ren, Journal of Electrochimica Acta 152 (2005) A1748.
[25] S.L. Chou, J.Z. Wang, D. Wexler, K. Konstantinov, C. Zhong, H.K. Liu, S.X. Dou, Journal of Materials Chemistry 20 (2010) 2092.

[26] Q. Zhang, M.Q. Zhao, D.M. Tang, F. Li, J.Q. Huang, B. Liu, W.C. Zhu, Y.H. Zhang, F. Wei, Angewandte Chemie International Edition 49 (2010) 3642.
[27] Q. Han, Z. Liu, Y. Xu, Z. Chen, T. Wang, H. Zhang, Journal of Physical Chemistry C 111 (2007) 5034.
[28] M. Aronniemi, J. Sainio, J. Lahtinen, Surface Science 578 (2005) 108.
[29] X. Jia, Z. Chen, Y. Peng, X. Wang, F. Wei, Y. Lu, ACS Nano 6 (2012) 9911–9919.
[30] X. Jia, Z. Chen, A. Suwarnasarn, L. Rice, X. Wang, H. Sohn, Q. Zhang, B.M. Wu, F. Wei, Y. Lu, Energy Environmental Science 5 (2012) 6845–6849.
[31] J. Huang, X. Liu, Q. Zhang, C. Chen, M. Zhao, S. Zhang, W. Zhu, W. Qian, F. Wei, Nano Energy 2 (2013) 314–321.

Guo Gao obtained his Ph.D. degree from the School of Chemical Engineering at Dalian University of Technology in 2007, China. After a postdoctoral fellowship from the School of Chemical Engineering at Tsinghua University, he was appointed as a lecturer in the Institute of Micro/Nano Science and Technology at Shanghai Jiao Tong University in 2009, and was appointed as an associate professor at Shanghai Jiao Tong University in 2011. His current research interests are advanced functional nanomaterials, multifunctional nanomaterials in biomedical engineering and energy conversion and storage.

Qiang Zhang graduated in 2004 from the Department of Chemical Engineering, Tsinghua University, China, where he continued doing research on mass production of carbon nanotubes and obtained his Ph.D. in chemical engineering in 2009. After a short stay as a research associate in Case Western Reserve University, USA in 2009, he joined the Fritz Haber Institute of the Max Planck Society, Germany as a post-doctoral fellow. He was appointed as an associate professor of chemical engineering in the Tsinghua University in 2011. His current research interests are nanocarbon, advanced functional materials, sustainable chemical engineering, energy conversion and storage.

Kan Wang obtained her Ph.D. in biomedical and engineering from The Forth Military Medical University in 2008, China. After a postdoctoral fellowship at Shanghai Jiao Tong University in 2008, she was appointed as a lecturer in the Institute of Micro/Nano Science and Technology of Shanghai Jiao Tong University in 2011. Her scientific interests are nanotechnology development of early cancer detection and screening equipment, nanomaterial molecular imaging and biocompatibility evaluation, and biological tissue impedance spectrum characteristics.

Hua Song obtained his Ph.D. in medicine from School of Pharmacy of Second Military Medical University and Shanghai University of T.C.M. in 2007, China. After a postdoctoral fellowship at School of Materials Science and Engineering of Shanghai Jiao Tong University, he was appointed as a lecturer in the Institute of Micro-Nano Science and Technology of Shanghai Jiao Tong University. He mainly focuses on the nano-drugs interdisciplinary research areas. His scientific interests include: the nanotechnology based targeted drug delivery system of antineoplastic; the nanotechnology based controlled release drug delivery system; the safety evaluation of nano-drugs and nano-materials; the synthesis and the molecular imaging evaluation of new nano-probe.

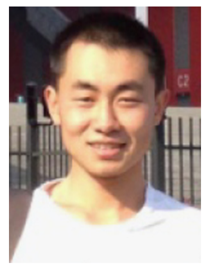

Peiyu Qiu was born in Jilin, China in 1990. He received his B.E. degree from University of Science and Technology, Beijing in 2012. Now, he is studying as M.E. candidate under the guidance of A/Prof. Guo Gao at Shanghai Jiao Tong University. His current research interests include magnetic nanoparticles and rare-earth luminescence nanomaterials.

Daxiang Cui obtained his Ph.D. in biochemistry and molecular biology from Fourth Military Medical University in China in 1998, was appointed as an associated professor in the Fourth Military Medical University in 2000, and professor in the Shanghai Jiao Tong university in 2004. He was a post-doc staff in the Max Planck Institute for Metals Research, and a visiting professor in the Waseda University. So far his interests focus on preparation of multifunctional nanomaterials and their application in biomedical engineering and energy.